ResearchGate

See discussions, stats, and author profiles for this publication at: https://www.researchgate.net/publication/231643259

Magnetic Transition and Large Magnetocaloric Effect Associated with Surface Spin Disorder in Co and CocoreAgshell Nanoparticles

ARTICLE *in* THE JOURNAL OF PHYSICAL CHEMISTRY C · SEPTEMBER 2007

Impact Factor: 4.77 · DOI: 10.1021/jp073274i

CITATIONS
23

READS
36

5 AUTHORS, INCLUDING:

Pankaj Poddar
CSIR - National Chemical Laboratory, Pune
129 PUBLICATIONS **2,427** CITATIONS
SEE PROFILE

Srinath S
University of Hyderabad
123 PUBLICATIONS **838** CITATIONS
SEE PROFILE

Prasad Blv
CSIR - National Chemical Laboratory, Pune
108 PUBLICATIONS **2,710** CITATIONS
SEE PROFILE

Available from: Pankaj Poddar
Retrieved on: 03 February 2016

ARTICLES

Magnetic Transition and Large Magnetocaloric Effect Associated with Surface Spin Disorder in Co and $Co_{core}Ag_{shell}$ Nanoparticles

P. Poddar,*,† S. Srinath,*,‡,§ J. Gass,‡ B. L. V. Prasad,† and H. Srikanth‡

Materials Chemistry Division, National Chemical Laboratory, Pune-411 008, India, Functional Materials Laboratory, Department of Physics, University of South Florida, Tampa, Florida-33620, and School of Physics, University of Hyderabad, Hyderabad-500046, Andhra Pradesh, India

Received: April 28, 2007; In Final Form: July 24, 2007

We report a reversible, large magnetocaloric effect in the vicinity of a low-temperature magnetic transition in Co and $Co_{core}Ag_{shell}$ nanoparticles synthesized using a wet chemical method. The as-synthesized assembly of the particles shows a sharp low-temperature peak in the zero-field-cooled (ZFC) magnetization well below the blocking transition temperature, and this feature is associated with the surface spin disorder. Co nanoparticles show a large increase in the magnetic entropy at around 15 K with a peak value of nearly 2.25 J/K·kg for an applied field of 30 kOe. A similar trend is also observed in the silver-coated Co particles. These are some of the largest MCE values observed in nanoparticles to date. The features are ascribed to the low-temperature spin-glass-like freezing transition associated with the surface spins in the shell region that is distinct from the behavior of core spins. Our studies reveal that manipulating the surface anisotropy in core−shell nanoparticles has the potential to lead to a large MCE effect and thus prove to be useful for magnetic refrigeration.

Introduction

Historically, magnetocaloric refrigeration was used to reach milli-Kelvin temperatures in paramagnetic salts by using adiabatic demagnetization.[1−3] The magnetocaloric refrigeration in bulk materials has been studied in manganites, intermetallic compounds, Gd, $Gd_5(Si_2Ge_2)$,[2,4] etc. Recently, considerable efforts have been made toward their high-temperature applications.[2,4] Giant magnetocaloric effect (MCE) has been mostly observed in bulk materials, such as $Gd_5(Si_2Ge_2)$, and is understood to be due to the magnetic field induced first-order structural transitions.[1] Although the observation of giant MCE is promising, most of the current bulk MCE materials rely on the entropy change associated with the paramagnetic−ferromagnetic transition at the Curie temperature. The MCE shows a maximum in the vicinity of the Curie temperature and drops off sharply on either side.[5,6] Additionally, these materials are difficult to be integrated with MEMS devices for local spot-cooling applications due to their inherent limitations in thin-film processing while maintaining the stoichiometric ratio and MCE properties. The field required for efficient cooling is also extremely high and can be normally reached only by using sophisticated and expensive superconducting magnets.

Magnetic nanoparticles provide an attractive alternative to the conventional bulk MCE materials because of their ease of assembly in thin-film forms and other desirable features such as control over the entropy change across the superparamagnetic-blocking transition usually determined by the particle size. It has been theoretically shown that by reducing the average particle size close to the single magnetic domain, the magnetic entropy change increases by several orders of magnitude as compared to the entropy change in bulk materials.[7] In addition, the large surface area in nanostructured materials has the potential to provide better heat exchange with the surrounding materials.[1] However, to prevent agglomeration of nanoparticles, MCE studies have been mainly focused on nanocomposites where nanoparticles such as Fe, Fe_3O_4 have to be dispersed in a matrix in order to prevent the agglomeration associated with the surface energy minimization. To date, not too many studies of the MCE in nanocomposites have been reported.[8−12] Even though these reports indicate an enhanced MCE due to the reduction of grain size to the nanoscale dimensions, the overall effect is quite low due to the fact that in such a nanocomposite material, the concentration of nanoparticles remains under 66% and the nonmagnetic inactive matrix acts as a heat sink.[12]

Recently, we have reported a comparative study of MCE in two different soft ferrite nanoparticle systems where the particles were synthesized with selective size range chosen to yield monodisperse and polydisperse materials.[13] We found that the entropy change in both systems was nearly constant over a broad temperature region; however, the overall entropy change value was 2−3 orders of magnitude lower than that reported for giant MCE materials. We also observed that the entropy change for the monodisperse system was comparatively larger than for the polydisperse system which is generally consistent with theoretical predictions and associated experimental results.[8,12,13]

Cobalt nanoparticles have attracted significant interest due to their technological significance and fundamental physics and

* Corresponding authors. E-mail: p.poddar@ncl.res.in (P.P.); sssp@uohyd.ernet.in (S.S.).
† National Chemical Laboratory.
‡ University of South Florida.
§ University of Hyderabad.

10.1021/jp073274i CCC: $37.00 © 2007 American Chemical Society
Published on Web 09/05/2007

have been investigated by a number of groups.[14−18] In the present work, in an effort to search for even larger magnetic entropy change, we have developed two different strategies involving core−shell structures. In the first approach, we have used the passivating organic surfactant layer as shell and monodisperse cobalt particles as core thereby increasing the active magnetocaloric content and also decreasing the effective mass of the nanocomposite. In the second approach, we have used a conductive shell in the form of Ag with Co as the magnetic core. In the latter case, the outer metallic Ag is expected to not only provide a desirable high thermal conducting surface but also prevent agglomeration and surface oxidation that tend to degrade magnetic and MCE properties. By careful design of core−shell structures in such a way, there is a better chance of controlling the heat exchange between the magnetic nanoparticles and the surrounding lattice. Our goal is also to obtain a fundamental understanding of the influence of surface environment and interparticle interactions on the overall magnetocaloric properties.

Results and Discussion

Synthesis of Co nanoparticles was performed by a simple, aqueous medium based wet chemical technique at ambient temperature with optimized concentration of a mixture of surfactants—sodium dodecyl sulfate (SDS) and oleic acid. The Co^{2+} ions were reduced by 0.05% $NaBH_4$. On the basis of the observations made with various concentration ratios of SDS and oleic acid, it is suggested that the formation of vesicles plays a crucial role in the formation and stability of these nanoparticles. The synthesis and characterization details are presented elsewhere.[19] A typical transmission electron microscopy (TEM) image of as-synthesized Co nanoparticles is presented in Figure 1a. Analysis of this and several other images reveals that the bulk of the particles have a mean size of ∼50 nm. The image also shows that the particles are well separated from each other presumably due to the surfactant coating. We used high-resolution TEM (HR-TEM) to further probe the crystallinity of the particles (results are presented in the Supporting Information as they are communicated in a separate paper[19]). An important point (with its broader implications on the X-ray diffraction results and the magnetic properties) to note here is that each spherical particle of mean size ∼50 nm is in fact a self-assembly of much smaller crystallites. Moreover, lattice spacing in each crystallite matches very well with the lattice spacing of the bulk Co materials which concludes that these smaller crystallites are pure in their crystalline phase. A third point to note here is that each spherical assembly of crystallites (mean size ∼50 nm) also contains a large area filled with amorphous material which may be due to the presence of surfactant or cobalt oxide in the amorphous form cobalt.[19] Although we cannot rule out the presence of these amorphous alloys on the surface of each of the small crystallites, the HR-TEM images clearly point to the presence of phase pure Co albeit in the form of very small crystallites.[19]

The X-ray diffraction (XRD) analysis of Co particles shows the presence of mixed fcc and tetragonal phases without any evidence for the CoO phase (results communicated separately[19]). However, as we indicated earlier, the presence of a thin surface layer of amorphous CoO cannot be ruled out. The XRD peaks are quite broad indicating that the actual crystallite size is much smaller (∼4 nm) in comparison to the predominant 50 nm particles seen in TEM which is in consistent with the HR-TEM result that points to the fact that as-synthesized particles are polycrystalline in nature where each crystallite size is much

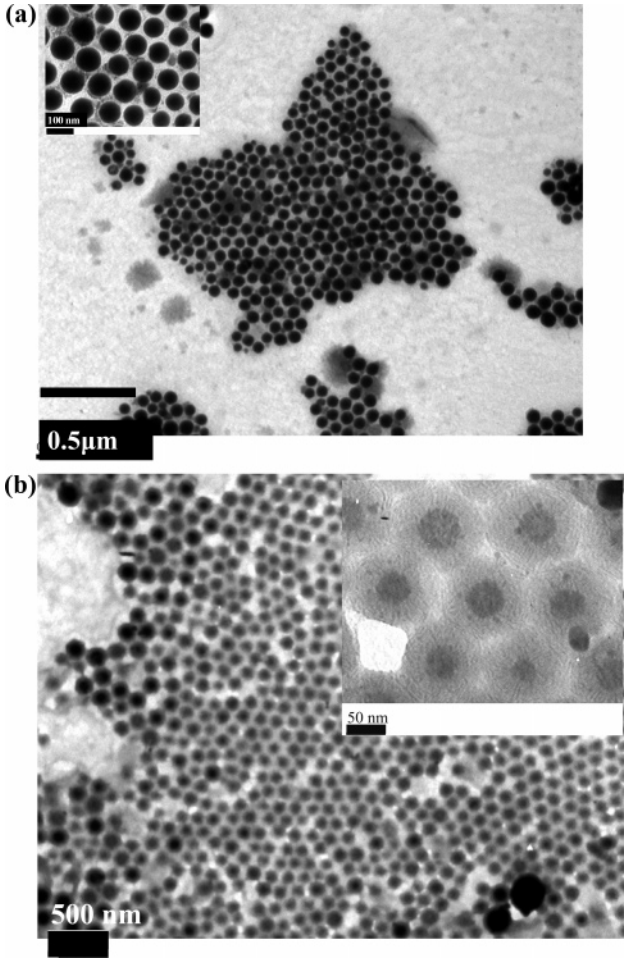

Figure 1. (a) TEM images of Co nanoparticles. The inset shows the zoom view. (b) TEM images of Co−Ag core−shell nanoparticles. The inset shows the zoom view.

smaller.[19] It is reported that the tetragonal phase is formed due to the dissolved oxygen which converts to the fcc phase after mild annealing.[19,20]

The $Co_{core}Ag_{shell}$ particles were synthesized by replacing the surface layer of Co (shown in Figure 1) with Ag using the transmetallation reaction.[19] For this reaction, the Co particles were stirred with silver salt using a magnetic stirrer. The reduction potential for Ag^+ is +0.80 V, whereas for Co^{2+} it is −0.28 V. The higher reduction potential of Ag^+ in comparison to Co^{2+} leads to replacement of each Co atom with two Ag atoms at the surface, thereby forming a core−shell structure. The transmetallation reaction can be represented as follows:

$$Co(s) + 2Ag^+(aq) \rightarrow 2Ag(s) + Co^{2+}(aq) \quad (\text{reduction potential} \approx 1.08\ \text{V}) \quad (1)$$

It should be noted here that before the transmetallation reaction, we extensively washed our initial Co particles, to remove any unreacted $NaBH_4$. Thereafter, the only possible way, in the absence of an external reducing agent, for Ag^+ to become Ag^0 is by the reaction $Co^0 + 2Ag^+ \rightarrow 2Ag^0 + Co^{2+}$ on the surface of Co nanoparticles leading to the core−shell morphology observed here, which is proved by UV−vis spectroscopy (results not presented here). Hence, we strongly believe that the core−shell particles we observe are of $Co_{core}Ag_{shell}$ morphology. After partial transmetallation, the overall size of the magnetic core reduces. TEM images in Figure 1b indicate that

the average core size is reduced to 40 nm and average shell thickness is ~28 nm. The transmetallation is essentially a surface phenomenon and has been utilized to generate completely hollow Au nanostructures replacing Ag ions out of Ag nanoparticles by Au[21] or other porous structures.[22−25] It is believed that in this process, the elemental silver is confined to the vicinity of the Co nanoparticle surface which acts as a template. The silver atoms nucleate and grow into very small particles and eventually evolve into a thin film around the Co nanoparticles.[22] The larger than expected thickness of the Ag shell is quite interesting. TEM images show that in contrast to the Co particles, the $Co_{core}Ag_{shell}$ nanoparticles are in contact with each other with the partial absence of the organic surfactant layer. This could be reconciled as follows. During the transmetallation reaction, surface Co atoms are replaced by Ag atoms, and in this process, the surfactant molecules which are bound to the Co atoms are also partially removed. It should also be noted that the TEM image of the core−shell nanoparticles shows a shiny shell around a dark core; however, the opposite is expected (i.e., a dark shell around a shiny core). The origin of this feature at this point is not understood completely, but a recent work by Chen et al. has also proved that the "shiny shells around a dark cores" are indeed $Ni_{core}Au_{shell}$ particles.[24b]

Magnetic characterization was done using a commercial 7 T physical property measurement system (PPMS) from Quantum Design. For the temperature- and field-dependent magnetization measurements, dried samples in powder form were packed into a gel cap and care was taken to enclose them tightly so that no mechanical motion of particles was possible under external fields. Standard zero-field-cooled (ZFC) and field-cooled (FC) measurements were done at an applied field of 100 Oe, and the hysteresis loop measurements were performed at 2 and at 300 K between −30 and 30 kOe field range. The MCE was extracted from a large set of $M-H$ curves collected at different fixed temperatures using a LABView-based module and subsequently analyzed. Experiments were repeated with different samples to check for reproducibility of the data.

The ZFC−FC curves for the surfactant-coated Co nanoparticles are shown in the top panel of Figure 2. The blocking transition peak (T_B) is located at around 135 K with superparamagnetic response at higher temperatures. The broad maximum seen in ZFC and the lower than expected blocking temperature for the average size of Co particles may be due to the presence of polycrystalline nature of Co nanoparticles as discussed above. It is remarkable to see here that instead each particle being an assembly of smaller crystallites (~5 nm), the overall ZFC−FC curve behaves as expected from much bigger particles (though smaller than 50 nm) which is due to strong exchange coupling between the crystallites. The estimated single-domain size based on the theories for the single-domain particles and bulk property values for Co spherical particles is 70 nm.[26] In general this value is affected by the high surface anisotropy and low saturation magnetization of the nanoparticles in comparison with the bulk. Another feature that is quite striking in the magnetization data is the anomaly seen at around 16 K with the ZFC magnetization displaying a sharp peak and the corresponding FC curve showing a sharp increase. Such transitions have been observed in the past, and we believe that this may originate from (1) the surface spins which can be considered to behave like a disordered spin glass[27−29] and/or (2) possible oxidation of surface Co atoms. To consider the first possibility—above 16 K, the surface spins will randomize even in the presence of a weak external field while the core spins are blocked, and as the temperature decreases, fine-particle blocking effects begin to dominate. This

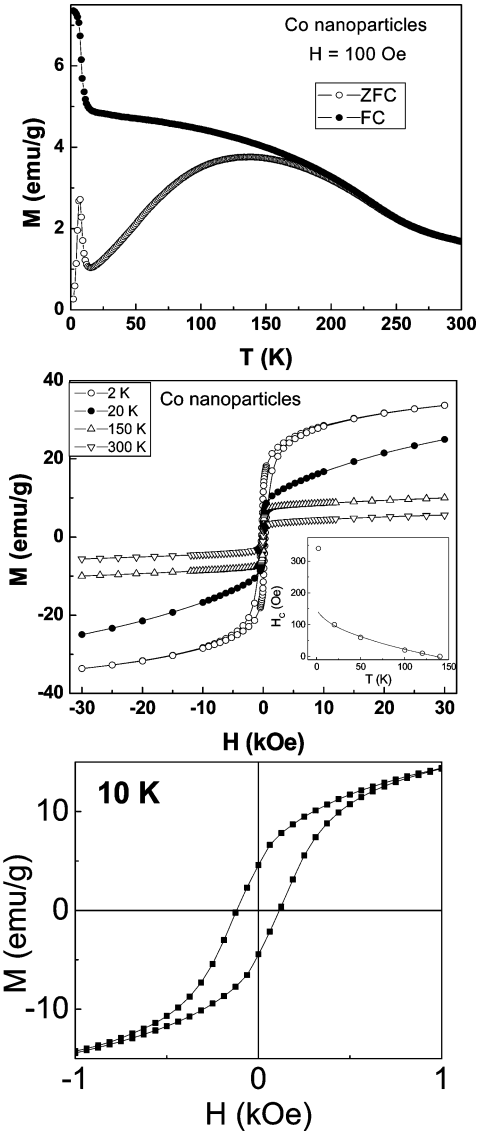

Figure 2. (Top panel) Field-cooled (FC) and zero-field-cooled (ZFC) curves for Co nanoparticles at 100 Oe. (Middle panel) Hysteresis loops of Co nanoparticles at different temperatures; Inset: temperature dependence of H_C along with the fit based on eq 2. (Bottom panel) $M-H$ loop at 10 K temperature showing the absence of exchange-bias type of shift.

argument is also validated by the fact that the FC magnetization shows a sharp increase as the surface spins are frozen in the field direction. The sharp rise in net moment near the peak temperature may in part be due to an increase in the moment per cobalt atom at the surface of the particle when the thermal activation energy is too small. This is followed by a sharp drop at lower temperature which is to be expected when the surface spins freeze with relatively random orientations (unlike the case of the FC curve where the external field introduces some alignment) resulting in a spin-glass-like short-range order. The low-temperature anomaly was also reproduced in the particles dispersed in wax thereby completely ruling out any role of physical movement of the particles. As we pointed out earlier, the presence of an amorphous Co_3O_4 layer at the surface may also cause this transition as it is in the vicinity of the Neel temperature of Co_3O_4 which is normally in a range from 25 to 40 K.

In the middle panel of Figure 2, we have shown the $M-H$ curves at 2, 20, 150, and 300 K. The curves at 150 and 300 K

show reversible behavior with no discernible coercivity, but the low-temperature data clearly shows opening up of the hysteresis loops with a coercivity (H_C) of ~340 Oe at the lowest temperature of measurement (2 K). None of these curves saturate at the highest applied field of 30 kOe which is consistent with the notion of unsaturated (disordered) surface spins as discussed above. The particles dispersed in wax also show similar $M-H$ loops at low temperatures ruling out the possibility of either physical rotation or movement of the sample in the gel cap. In the bottom panel, we have shown the zoom view of the $M-H$ curve at 10 K which shows a very symmetric curve with coercive field of ±120 Oe (both sides). The absence of any asymmetry rules out any presence of exchange-bias type of feature due to any cobalt oxide phase in our material.

The $H_C(T)$ values at different temperatures are shown in the inset of the middle panel of Figure 2. For the noninteracting, randomly oriented, single-domain particles with uniaxial anisotropy, the coercive field $H_C(T)$ at temperature T is given by the following relation:

$$H_C(T) = H_C(0)\left[1 - \left(\frac{T}{T_B}\right)^{1/2}\right] \quad (2)$$

where $H_C(0) = 0.64K/M_S$; M_S is the saturation magnetization, and K is the effective anisotropy which is a combination of magnetocrystalline anisotropy (field required to saturate the magnetization in the hard direction), shape anisotropy, surface anisotropy, etc.[30] This equation clearly shows that coercivity is directly proportional to the anisotropy constant and inversely proportional to the saturation magnetization. The solid line in the middle panel of Figure 2 is the fit obtained based on eq 2. It can be seen that temperature dependence of H_C can be very well described in the temperature range of 10−140 K (below T_B) giving $H_{CO} \sim 158$ Oe and $T_B \sim 135$ K. The T_B obtained from this fit matches very well with the blocking transition peak observed in ZFC magnetization (Figure 1). However, there is a sudden increase in H_C below 10 K, and at 2 K it has a large value ~340 Oe. The sharp increase in H_C is coupled with the low-temperature anomaly and can be explained due to the freezing of the surface spins. The increase in H_C is the same both when the particles are cooled in zero-field and also cooled in a large field of 5 T. The effective anisotropy from the M_S and the value of H_{CO} obtained from the above fit is $\sim 7.1 \times 10^4$ erg/cc. The increase in H_C at 2 K also suggests that the surface anisotropy increases considerably at low temperatures.

The magnetic entropy across any order−disorder transition can be obtained from the family of $M-H$ curves recorded at temperatures spanning the transition. The usual convention behind MCE is to associate cooling with the demagnetization cycle when the spins change from an ordered to a disordered state as the field is removed. The top panel of Figure 3 shows the $M-H$ curves for Co nanoparticles over a field range of 0−3 T taken at temperature intervals of 2 K from 2 to 30 K and at 5 K intervals up to 195 K which spans both the low-temperature peak as well as the blocking peak at higher temperature. The bottom panel shows the $M-T$ curves which is just plotting the data in the top panel in a different way.

A simple picture that emerges from our data is the distinctly different magnetic response of the core and shell regions. The total magnetization of each particle may be considered as consisting of two parts—the core magnetic moment (which is ordered and behaves as a superspin) and the shell magnetization (which is disordered and very similar to spin-glass systems). The exchange coupling between the surface and core spins can

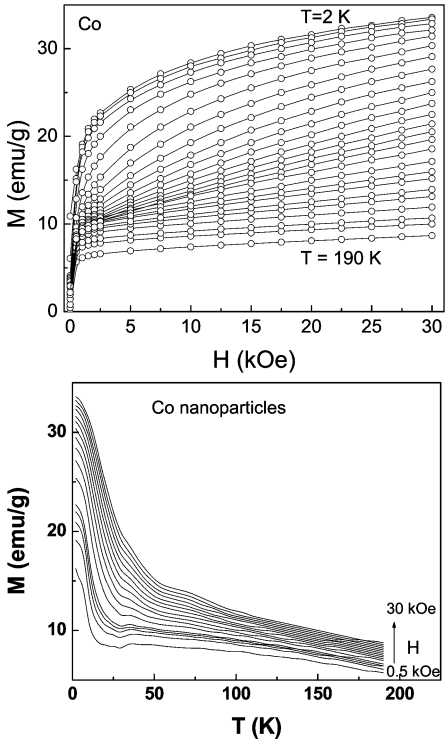

Figure 3. (Top panel) Isothermal curves of magnetization vs field ($M-H$). (Bottom panel) Same magnetization vs temperature curves as obtained from the $M-H$ curves.

lead to short-range order of the surface spins below a certain temperature with the surface anisotropy also competing in this process. The enhancement of the saturation magnetization at low temperatures can be due to the progressive short-range ferromagnetic ordering of the particle surface spins. Even though the steep increase in ZFC and FC magnetization is observed in many nanoparticle systems and has been attributed to the surface spin effects,[29] to our knowledge, there is no rigorous theory of magnetization that has considered the effect of coupling and decoupling of surface and core spins.

From the $M-H$ data, the entropy change in a magnetic system can be calculated from the thermodynamic Maxwell relation:

$$\left(\frac{\partial S}{\partial H}\right)_T = \left(\frac{\partial M}{\partial T}\right)_H \quad (3)$$

or integrating over the field,

$$\Delta S = \int_0^H \left(\frac{\partial M}{\partial T}\right)_H \mathrm{d}H \quad (4)$$

In Figure 4, we have presented the entropy change (ΔS) versus temperature for Co nanoparticles for a field change from 0 to 10 kOe, 0 to 20 k Oe and 0 to 30 k Oe. As evident from Figure 4, the magnetic entropy change is negative (i.e., heating of the system while applying the magnetic field and cooling of the system while removing the field. The convention is that demagnetization cycle will result in cooling of the surrounding lattice). The overall entropy change increases with increased change in the magnetic field as expected. A notable feature that can be observed is that instead of observing the maximum of entropy change in the vicinity of the blocking temperature, a sharp peak is located at the low-temperature magnetization peak discussed earlier. In the case of nanoparticles, we have observed previously that the maximum change in the entropy is normally

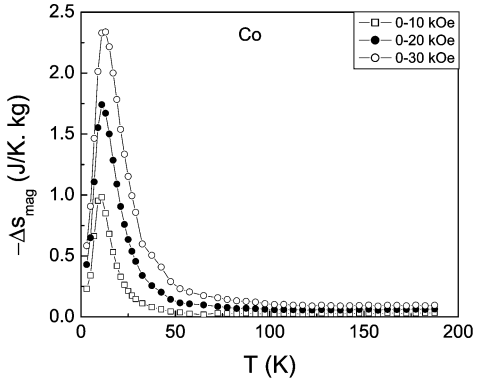

Figure 4. Magnetic entropy change vs temperature curves at various magnetic field values for Co nanoparticles.

located above the blocking temperature transition.[13] However, in this system we do not see such an effect, and this is likely due to the dominance of the surface effects rather than the core nanoparticle response. To investigate it further, we performed magnetic measurements as well as magnetic entropy calculations for another system where Co is replaced by Ni. For the case of Ni nanoparticles and Ni−Ag core−shell nanoparticles, synthesized by following the same protocol, we did not observe the low-temperature anomaly and instead observed a change in the magnetic entropy above the blocking temperature. The results on Ni nanoparticles are not discussed here and will be the focus of a separate manuscript under preparation.

In the top panel of Figure 5, we have shown the ZFC−FC curves for the $Co_{core}Ag_{shell}$ nanoparticles. For this system, the blocking temperature is located at around 150 K which is higher in comparison to that of Co particles (135 K). In principle, the shell formation should result in a reduced magnetic core volume, which should lower the blocking temperature.[18] However, an increase in the blocking temperature after the coating points toward enhanced surface anisotropy for $Co_{core}Ag_{shell}$ nanoparticles in comparison to Co nanoparticles with organic surfactant. Additionally, in Figure 5, the low-temperature anomaly, which was around 16 K in the case of Co particles, is also shifted to 27 K. In the middle panel of Figure 5, the $M-H$ loops measured at 2, 10, and 300 K are presented. While comparing the curves for Co and $Co_{core}Ag_{shell}$ particles, we observed that at 10 K the magnetization at 30 kOe for Co particles is larger (∼31.5 emu/g) than that for $Co_{core}Ag_{shell}$ particles (∼30 emu/g) which is consistent with the reduction in the core size for the latter. The curve at 2 K (bottom panel) shows a coercivity of 500 Oe for the $Co_{core}Ag_{shell}$ particles which is larger than the coercivity for Co particles (340 Oe). The enhanced coercivity for the core−shell particles supports the previous observations of increased blocking temperature and increased effective anisotropy. Again, any absence of shift in the coercive field shows absence of any exchange-bias type of behavior.

As discussed above on the basis of the TEM image, $Co_{core}Ag_{shell}$ particles are most likely to have less molecules of the organic surfactant at the surface which will lead to the particles physically in contact. The presence of the metal−ferromagnet interface favors the RKKY mechanism wherein long-range indirect interactions in moments are mediated by the conduction electrons.[31] In the present case, we believe that due to the large thickness of the shell (∼28 nm) the RKKY interaction occurs only in the proximity of the interface and drops off further into the shell region. The effect of systematic variation of the metal shell thickness and the influence on magnetic properties would be interesting in the context.

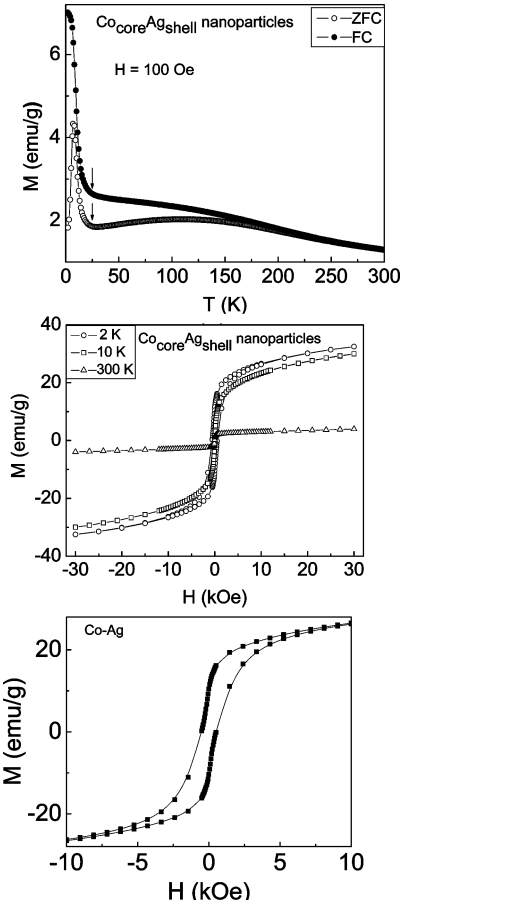

Figure 5. (Top panel) Field-cooled (FC) and zero-field-cooled (ZFC) curves for Co−Ag core−shell nanoparticles at 100 Oe. (Middle panel) Hysteresis loops of Co−Ag core−shell nanoparticles at different temperatures. (Bottom panel) Zoom view of the $M-H$ loop at 2 K showing the symmetrical nature of the loop (absence of exchange-bias type of shift).

The top panel of Figure 6 shows the $M-H$ curves for $Co_{core}Ag_{shell}$ nanoparticles over a field range of 0.5−3 T taken at temperature intervals of 10 K from 5 to 195 K. The bottom panel shows the $M-T$ curves as obtained from the top panel. In Figure 7, we have presented the magnetic entropy change as calculated from the $M-T$ curves presented in Figure 6 using eq 2. It can be noticed from this figure that the entropy change versus temperature curves show a sharp peak at around 20 K. In fact, for higher field change (0−30 kOe), the peak shifts slightly toward higher temperatures as also seen for Co nanoparticles. The large MCE observed in these systems coincides with the anomalies observed at low temperature indicating again the role of surface anisotropy. In Table 1, we have compared the change in the magnetic entropy of Co and $Co_{core}Ag_{shell}$ nanoparticles at various magnetic fields and temperature values.

The results presented above show that even after replacing the Co atoms at the surface by Ag atoms by transmetallation, the disorder of spins persist. In fact, from the MCE perspective the effect of the order−disorder transition is even enhanced in these metal shell−magnetic core systems when compared with organic insulator−magnetic core systems. It is obvious that in both cases the core is Co and the only difference is the shell environment. We have shown in the past that the influence of even two different organic, insulating surfactants has an effect on the magnetic properties of nanoparticles.[32] So it is not surprising that the presence of a metallic Ag layer does appear

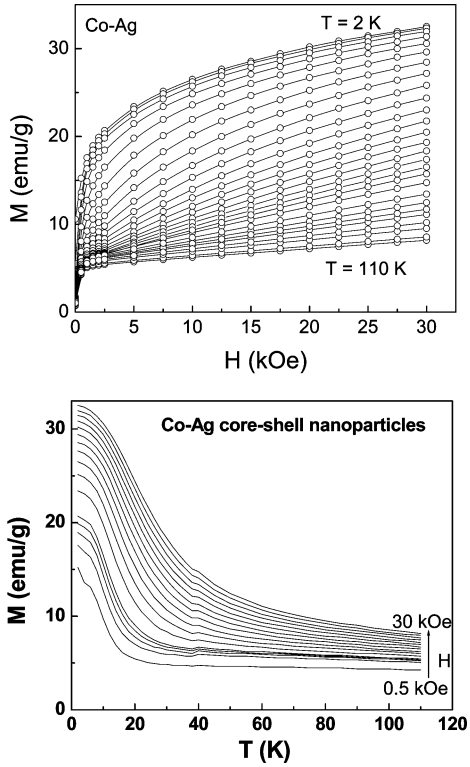

Figure 6. (Top panel) Isothermal curves of magnetization vs field ($M-H$) for the same. (Bottom panel) Same magnetization vs temperature curves as obtained from the $M-H$ curves.

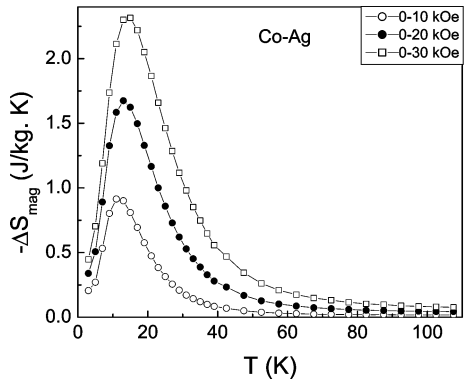

Figure 7. Magnetic entropy change vs temperature curves at various magnetic field values for Co−Ag core−shell nanoparticles.

TABLE 1: Comparison of Change in the Magnetic Entropy of Co and $Co_{core}Ag_{shell}$ Nanoparticles at Various Magnetic Fields and Temperature Values[a]

	applied field					
	$H = 10$ kOe		$H = 20$ kOe		$H = 30$ kOe	
temp K	Co	$Co_{core}Ag_{shell}$	Co	$Co_{core}Ag_{shell}$	Co	$Co_{core}Ag_{shell}$
8	−0.66	−0.66	−1.11	−1.10	−1.46	−1.47
13	−0.91	−0.89	−1.70	−1.66	−2.35	−2.28
18	−0.53	−0.64	−1.28	−1.41	−2.00	−2.13

[a] All the values of the magnetic entropy in the table are in the units of J/K·kg.

to have a profound effect on the surface environment and consequently on blocking temperature and MCE. The role of the metal capping layer on surface spin disorder is unknown at present, and our observations could be of interest for further theoretical interpretation.

Finally, we would like to point out that the magnetic entropy values obtained in this work are 2 orders of magnitude greater than has been reported on any nanoparticle system so far although the large values are in the vicinity of the low-temperature transition. This is due to the strong surface anisotropy that these particles exhibit at low temperatures as evidenced by the low-temperature anomaly and a sharp increase in H_C.

Conclusions

We have observed a surface spin order−disorder transition at low temperature and an associated large MCE in Co and $Co_{core}Ag_{shell}$ nanoparticles. Our studies categorically show that one should not dismiss nanoparticle-based magnetic systems as not having the potential to match up with bulk giant MCE alloys. Our work, for the first time, opens up the possibility of controlling surface anisotropy and possibly even the exchange coupling at the core−shell interface in nanoparticle-based systems that could lead to promisingly high MCE parameters useful for refrigeration applications.

Acknowledgment. NCL authors acknowledge the NCL in-house Grant: MLP 007026 and the DST Grant for setting up a Unit on Nano Science and Technology (DST-UNANST) at NCL. Work at USF is supported by NSF through Grant No. CTS-0408933 and ARO through Grant No. W911NF-05-1-0354.

Supporting Information Available: HR-TEM images of Co particles. This material is available free of charge via the Internet at http://pubs.acs.org.

References and Notes

(1) Giauque, W. F.; MacDougall, D. P. *Phys. Rev.* **1933**, *43*, 768.
(2) Gschneidner, K. A., Jr.; Pecharsky, V. K. V. K.; Tsokol, A. O. *Rep. Prog. Phys.* **2005**, *68*, 1479.
(3) Pecharsky, V. K.; Gschneidner, K. A., Jr. *Phys. Rev. Lett.* **1997**, *78*, 4494.
(4) Bohigas, X.; Tejada, J.; del Barco, E.; Zhang, X. X.; Sales, M. *Appl. Phys. Lett.* **1998**, *73*, 390.
(5) *Nanoscale Materials in Chemistry*; Klabunde, K. J., Ed.; John Wiley and Sons, Inc.: New York, 2001.
(6) Pecharsky, V. K.; Gschneidner, K. A., Jr. *J. Magn. Magn. Mater.* **1999**, *200*, 44.
(7) McMichael, R. D.; Schull, R. D.; Swartzendruber, L. J.; Bennett, L. H.; Watson, R. E. *J. Magn. Magn. Mater.* **1992**, *111*, 29.
(8) (a) Yamamoto, T. A.; Tanaka, M.; Misaka, Y.; Nakagawa, T.; Nakayama, T.; Niihara, K.; Numazawa, T. *Scr. Mater.* **2002** *46*, 89. (b) Tanaka, M.; Misaka, Y.; Shiomi, K.; Yamamoto, T. A.; Nakagawa, T.; Katsura, M.; Numazawa, T.; Nakayama, T.; Niihara, K. *Scr. Mater.* **2001**, *44*, 2141.
(9) Yamamoto, T. A.; Tanaka, M.; Nakayama, T.; Nishimaki, K.; Nakagawa, T.; Katsura, M.; Niihara, K. *Jpn. J. Appl. Phys.* **2000**, *39*, 4761.
(10) Provenzano, V.; Li, J.; King, T.; Canavan, E.; Shirron, P.; Dipirro, M.; Shull, R. D. *J. Magn. Magn. Mater.* **2003**, *266*, 185.
(11) Hueso, L. E.; Sande, P.; Miguens, D. R.; Rivas, J.; Rivadulla, F.; Lopez-Quintela, M. A. *J. Appl. Phys.* **2002**, *91*, 9943.
(12) Kinoshita, T.; Seino, S.; Muruyama, H.; Otome, Y.; Okitsu, K.; Nakayama, T.; Niihara, K.; Nakagawa, T.; Yamamoto, T. A. *J. Alloys Compd.* **2004**, *365*, 281.
(13) Poddar, P.; Gass, J.; Rebar, D. J.; Srinath, S.; Srikanth, H.; Morrison, S. A.; Carpenter, E. E. *J. Magn. Magn. Mater.* **2006**, *307*, 227.
(14) McHenry, M. E.; Majetich, S. A.; Artman, J. O.; DeGraef, M.; Stanley, S. W. *Phys. Rev. B* **1994**, *49*, 11358.
(15) (a) Chen, J. P.; Sorensen, C. M.; Klabunde, K. J.; Hadjipanayis, G. C. *Phys. Rev. B* **1995**, *51*, 11527. (b) Skumryev, V.; Stoyanov, S.; Zhang, Y.; Hadjipanayis, G.; Givord, D.; Nogues, J. *Nature* **2003**, *423*, 850.
(16) (a) Puntes, V. F.; Krishnan, K. M.; Alivisatos, A. P. *Science* **2001**, *291*, 2115. (b) Puntes, V. F.; Krishnan, K. M. *IEEE Trans. Magn.* **2001**, *37*, 2210.

(17) (a) Held, G. A.; Grinstein, G.; Doyle, H.; Sun, S.; Murray, C. B. *Phys. Rev. B* **2001**, *64*, 012408. (b) Kortright, J. B.; Hellwig, O.; Chesnel, K.; Sun, S.; Fullerton, E. E. *Phys. Rev. B* **2005**, *71*, 012402.

(18) Zheng, R. K.; Hongwei, G.; Bing, X.; Zhang, X. X. *Phys. Rev. B* **2005**, *72*, 014416.

(19) Sidhaye, D. S.; Bala, T.; Srinath, S.; Srikanth, H.; Poddar, P.; Sastry, M.; Prasad, B. L. V. *J. Colloids Interface Sci.*, submitted.

(20) (a) Roy, A.; Srinivas, V.; Ram, S.; Toro, J. A. D.; Mizutani, U. *Phys. Rev. B* **2005**, *71*, 184443. (b) Roy, A.; Srinivas, V.; Ram, S.; Toro, J. A. D.; Riviero, J. M. *J. Appl. Phys.* **2004**, *96*, 6782.

(21) Sun, Y.; Mayers, B. T.; Xia, Y. *Nano Lett.* **2002**, *2*, 481.

(22) Mandal, S.; Selvakannan, P. R.; Pasricha, R.; Sastry, M. *J. Am. Chem. Soc.* **2003**, *125*, 8440.

(23) Sun, Y.; Xia, Y. *J. Am. Chem. Soc.* **2004**, *126*, 3892.

(24) (a) Bala, T.; Bhame, S. D.; Joy, P. A.; Prasad, B. L. V.; Sastry, M. *J. Mater. Chem.* **2004**, *14*, 2941. (b) Chen, D.; Li, J.; Shi, C. ; Du, X.; Zhao, N.; Sheng, J.; Liu, S. *Chem. Mater.* **2007**, *19*, 3399.

(25) Kodama, R. H.; Berkowitz, A. E.; McNiff, E. J.; Foner, S. *Phys. Rev. Lett.* **1996**, *77*, 394.

(26) Leslie-Pelecky, D. L.; Rieke, R. D. *Chem. Mater.* **1996**, *8*, 1770.

(27) Iglesias, O.; Labarta, A. *Phys. Rev. B* **2001**, *63*, 184416.

(28) Garanin, D. A.; Kachkachi, H. *Phys. Rev. Lett.* **2003**, *90*, 065504.

(29) (a) De Biasi, E.; Ramos, C. A.; Zysler, R. D.; Romero, H. *Phys. Rev. B* **2002**, *65*, 144416. (b) Winkler, E.; Zysler, R. D.; Mansilla, M. V.; Fiorani, D. *Phys. Rev. B* **2005**, *72*, 132409.

(30) (a) Sahoo, Y.; He, Y.; Swihart, M. T.; Wang, S.; Luo, H.; Furlani, E. P.; Prasad, P. N. *J. Appl. Phys.* **2005**, *98*, 054308. (b) Bozorth, R. M. *Ferromagnetism*; D. Van Nostrand: Princeton, NJ, 1956; Chapter 18, p 831.

(31) Fonda, E.; Teixeira, S. R.; Geshev, J.; Bobonneau, D.; Pailloux, F.; Traverse, A. *Phys. Rev. B* **2005**, *71*, 184411.

(32) Poddar, P.; Srikanth, H.; Morrison, S. A.; Carpenter, E. E. *J. Magn. Magn. Mater.* **2005**, *288*, 443.